Generalization of the Kantorovich Method of Dimensional Reduction

Dr. Krishnan Suresh
Department of Mechanical Engineering
University of Wisconsin, Madison
suresh@engr.wisc.edu

ABSTRACT

Boundary value problems posed over thin solids are often amenable to a dimensional reduction in that one or more spatial dimensions may be eliminated from the governing equation. One of the popular methods of achieving dimensional reduction is the Kantorovich method, where based on certain *a priori* assumptions, a lower-dimensional problem over a 'mid-element' is obtained. Unfortunately, the mid-element geometry is often disjoint, and sometimes ill defined, resulting in both numerical and automation problems.

A natural generalization of the mid-element representation is a *skeletal representation*. We propose here a generalization of the Kantorovich method that exploits the unique topologic and geometric properties of the skeletal representation. The proposed method rests on a quasi-disjoint Voronoi decomposition of a domain induced by its skeletal representation. The generality and limitations of the proposed method are discussed using the Poisson's equation as a vehicle.

Keywords: Geometric simplification, medial axis transforms, dimensional reduction, plate theory, CAD/ CAE.

1. INTRODUCTION

Engineering analysis typically entails solving boundary value problems via computational procedures such as the finite element method. When the underlying geometry is relatively thin, boundary value problems are amenable to a dimensional reduction in that one or more spatial variables may be eliminated from the governing equation, prior to a finite element discretization. This results in significant computational gains with minimal loss in accuracy [Donaghy 96]. A popular means of achieving dimensional reduction is the *Kantorovich method* [Kantorovich 64], [Pilkey 94], [Shames 85]. The essential aspects of the method are summarized below for the Poisson's equation. This summary will also help identify an important limitation of the method that we address here.

1.1 The Kantorovich Method

Consider a thin rectangular domain illustrated in Figure 1-1, where $h << l$. Let $U(x,y)$ be a field that satisfies the Poisson's equation:

$$\nabla^2 U + k = 0 \quad \text{for } (x,y) \in \text{interior}$$

$$\textit{Subject to: } U = 0 \quad \text{for } (x,y) \in \text{boundary}$$

The problem of determining $U(x,y)$ is two-dimensional, but since $h << l$ it may be reduced to an approximate one-dimensional problem via the Kantorovich method.

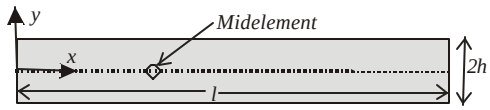

Figure 1-1: Mid-element of a rectangle.

The first step in the Kantorovich method is to express the Poisson's equation as an equivalent variational statement [Reddy 84], [Shames 85]:

$$\textit{Minimize } \Pi(U) = \frac{1}{2}\int_0^l \int_{-h}^{h} \left(U_{,x}^2 + U_{,y}^2 - 2kU\right) dy dx \qquad \textbf{(1-1)}$$

$$\textit{Subject to: } U = 0 \quad \text{for } (x,y) \in \text{boundary}$$

The next step is to seek an approximate solution $\hat{U}(x,y)$ that satisfies the boundary conditions on the 'dominant parallel edges', i.e., on $y = \pm h$. A non-trivial function satisfying this requirement is:

$$\hat{U}(x,y) = \left[1 - \left(\frac{y}{h}\right)^2\right] u(x)$$

Higher-order polynomials in y or even trigonometric functions may be used, provided $\hat{U}(x,\pm h) = 0$. $\hat{U}(x,y)$ is referred to here as a *Kantorovich trial function*; it defines the 'function space' in which a solution is being sought. Note that $\hat{U}(x,0) = u(x)$ where $u(x)$ is an unknown function over the line-segment $y = 0$. This line-segment is incidentally called a *mid-element* of the rectangle.

In the assumed function space, one can find $u(x)$ by substituting the trial function in the variational statement and integrating over y, i.e., eliminating y. This results in:

$$\textit{Minimize } \Pi(u,u_{,x}) = \int_0^l \left[\frac{16hu_{,x}^2}{15} + \frac{8u^2}{3h} - \frac{4khu}{3} \right] dx$$

Subject to: $u = 0$ for $x = 0, l$

Thus a 2-D variational problem has been reduced to a 1-D variational problem over the mid-element involving $u(x)$. One can now proceed to minimize the 1-D problem using standard 1-D finite element techniques [Reddy 84], [Shames 85].

Thus the above Kantorovich method may be viewed as a two-stage approximation process as opposed to a single stage finite-element method, as illustrated in Figure 1-2 [Babuska 94].

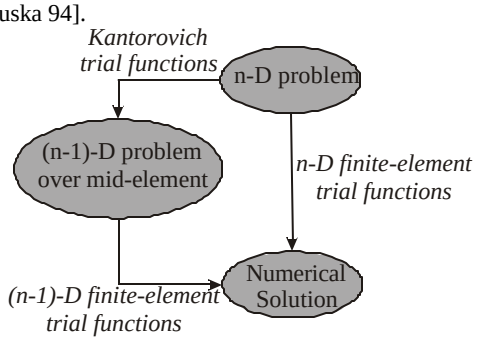

Figure 1-2: Mid-element dimensional reduction.

By considering Kantorovich trial functions that completely span the solution space, a hierarchical system of solutions $\hat{U}_n(x,y)$ that converge to the exact solution may be obtained; see hierarchical methods proposed by Babuska and others [Vogelius 81], [Babuska 94]. The two-stage approximation results in considerable computational gains since the first stage is executed once in a symbolic sense.

Various lower-dimensional theories of beams and plates are derived along similar lines. The starting point for such theories is the principle of virtual displacement, a generalization of the above variational statement, which states that for a system in static equilibrium, the work done by a virtual displacement must be zero [Shames 85]:

$$\int_V s_{ij} \delta e_{ij}\, dV - \int_V f_i \delta u_i\, dV - \int_{S_2} \hat{t}_i \delta u_i\, dD = 0$$

If the solid is sufficiently thin, one may assume certain trial functions for the displacements u_i, and a spatial variable may be eliminated resulting in a lower dimensional problem over the *mid-element* [Shames 85], [Wang 00].

2. LIMITATIONS OF THE MID-ELEMENT BASED KANTOROVICH METHOD

We now identify a serious drawback of the mid-element based Kantorovich method. Consider the notched rectangle illustrated in Figure 2-1. For simplicity, we shall assume that a field defined over the solid satisfies, as before, the Poisson equation and zero Dirichlet conditions.

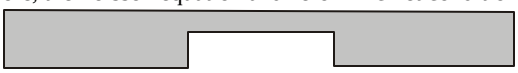

Figure 2-1: A notched rectangle.

Recall that, in the Kantorovich method, one must seek a trial function that satisfies the boundary conditions along the 'dominant parallel edges'. Due to the irregularity of the solid, it is not possible to define a single analytic function over the entire domain that meets this requirement. The domain is therefore divided into 3 quasi-disjoint regions Ω_1, Ω_2 and Ω_3 as illustrated in Figure 2-2. Further one can define a mid-element M_i and a thickness $2h_i$ with each region. The pairs (M_i, h_i) constitute the *mid-element representation* of the solid that unambiguously captures the geometry of the notched rectangle.

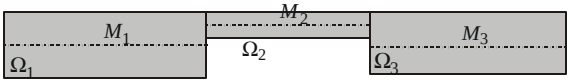

Figure 2-2: Mid-element based decomposition.

Observe that, due to the decomposition, the variational statement of Equation (1-1) can now be expressed as:

$$\textit{Minimize } \sum_{i=1}^{3} \frac{1}{2} \int_{0}^{l_i} \int_{-h_i}^{h_i} \left(\hat{U}_{i,x}^2 + \hat{U}_{i,y}^2 - 2k\hat{U}_i \right) dy_i\, dx_i$$

where the x-axis conveniently coincides with the mid-element M_i. We now define three trial functions $\hat{U}_1, \hat{U}_2$ and $\hat{U}_3$, one in each of the three domains per:

$$\hat{U}_i(x_i, y_i) = \left[1 - \left(\frac{y_i}{h_i} \right)^2 \right] u_i(x_i)$$

Observe that $\hat{U}_i(x_i, \pm h_i) = 0$, and $\hat{U}_i(x_i, 0) = u_i(x_i)$ where $u_i(x_i)$ are unknown functions.

With these definitions in place, one can eliminate y_i as before by substituting the assumed trial functions in the above variational formulation. This results in a variational statement governing three unknown functions u_i over the 3 independent mid-elements M_i.

At first glance, it appears that the above formulation is no different from that associated with a rectangle. However, this is not true … we have now violated the *admissibility criterion* of a variational formulation! It is a well-established fact that in a variational formulation, whenever a domain is sub-divided, and different trial functions are defined over each sub-domain, the trial functions must satisfy an *admissibility* criterion [Strang 73]. The admissibility criterion states that if the variational statement involves derivatives up to order m, then the trial functions must be at least C^{m-1} continuous across the boundaries of adjacent sub-domains.

In our case the variational statement involves only the first derivative of $U(x,y)$. *However, one can easily verify*

that the assumed trial functions $\hat{U}_i(x,y)$ *are not* C^0 *continuous across the common boundaries, violating the admissibility criterion*. This fact is often ignored, leading to both automation and numerical problems.

Since the assumed trial functions are *not admissible* from a variational standpoint, any attempt to couple the three functions u_1, u_2 and u_3, and their derivatives is necessarily *ad hoc* and approximate … it does not follow from the mid-element based geometric decomposition. More importantly, since the admissibility criterion is violated, no formal claims can be made about the convergence or accuracy of the mid-element based Kantorovich method, as it applies to such solids.

Further, a mid-element based decomposition does not always exist since the mid-element representation is incomplete for a large class of solids. For example, consider a dovetail section illustrated in Figure 2-3. Since there exists no mathematical definition of a mid-element, we rely on the dimensional reduction process to yield appropriate mid-elements. This would yield the mid-elements illustrated in Figure 2-3. However, it is now impossible to assign a thickness – even a varying one – to each of the mid-elements such that the solid may be recovered, i.e., the mid-element representation is incomplete. The two problems identified above are much more pronounced and difficult to resolve in 3-D.

Figure 2-3: Disjoint mid-elements for a dovetail

2.1 Prior Work

The Kantorovich method (and its variations) has been extensively investigated, as it applied to uniform-thickness plates and shells. The works of Reissner, Hencky, Mindlin, Lo, Reddy and others (see references in [Reissner 85]) fall into this category, so does the modern work on hierarchical modeling [Vogelius 81], [Babuska 91], [Madureira 99].

However, focusing our attention on geometrically more complex but thin solids, Armstrong and colleagues [Armstrong 94], [Donaghy 96] were the first to propose the use of *medial axis transform* (defined below) to resolve some of the geometric issues associated with the mid-element representation. The medial axis transform, or skeletal representation as it is referred to in this paper, is a natural generalization of the mid-element representation, and it consists of a skeleton and a radius function, where the skeleton 'follows' the shape of the solid, while the radius function captures the local thickness. The skeleton of the dovetail is illustrated in Figure 2-4. Observe the similarities and differences between Figure 2-3 and Figure 2-4. The most important difference is that the skeletal representation is *an unambiguous and complete geometric representation*, whose mathematical properties are now well understood [Choi 97], [Sherbrooke 96], and its role in engineering analysis is well documented [Tam 91], [Armstrong 95], [Price 95], [Armstrong 98], [Monaghan 98], [Sheffer 98], [Armstrong 99], [Shim 01].

Figure 2-4: The skeleton of the dovetail.

Since the skeletal representation of a solid is well defined, numerous authors [Donaghy 96], [Onodera 01] have proposed computing an approximate mid-element from the skeleton. However, the approximation involves heuristics since the mid-element is not mathematically well defined. Moreover, the resulting mid-element is not necessarily continuous, leading to a violation of the aforementioned admissibility criterion. Finally, there is an inherent loss in geometric information during the approximation. This loss can never be recovered in that the computed field solution will never converge to the exact solution in the sense of [Babuska 94].

In this paper, we propose a direct skeletal representation based Kantorovich method that does not rely on heuristics, and can therefore be fully automated. Further, the proposed method will not only satisfy the admissibility criterion, but also the *conformance criterion* [Strang 73], and is therefore expected to converge to the exact solution.

2.2 Skeletal Representation Based Generalization of the Kantorovich Method

The method proposed here combines the Kantorovich principle of two-stage reduction with the unique topologic and geometric properties of the skeletal representation, and has three essential features.

- First is the decomposition of a solid into its *S-Voronoi decomposition* (see Section 3).
- Second is the definition of *generalized Kantorovich trial functions* defined over the decomposition. By construction, the trial functions will not only satisfy the admissibility criterion, but will also be *complete* and satisfy *essential* boundary conditions.
- Third is the elimination of one of the space variables (essentially, the thickness parameter), by appropriate mathematical transformations.

In Section 3, we review the properties of skeletal representations. In Section 4, we describe the proposed method in detail using the Poisson's equation as a vehicle. In Section 5, numerical experiments involving Poisson problems over 2-D polygonal solids are presented. In Section 6, we propose a strategy for inclusion of singularities, and Section 7 summarizes the main contributions of the paper.

3. SKELETAL REPRESENTATIONS

Skeletal representations (s-reps) are characterized by two entities, namely a *skeleton (or medial axis)* and a *radius function.* The two entities are defined through the concept of a maximal ball [Sherbrooke 96]:

- A **closed ball** $B(p,r) \subset \Re^n$ is the set of points q such that $\|p-q\| \le r$

- A closed ball $B(p,r) \subset \Re^n$ is **maximal** with respect to Ω if it is contained in Ω, but not in any other closed ball contained in Ω.
- **Skeleton** of Ω is the locus of the centers of all maximal balls of Ω, plus the limit points of the locus.
- **Radius function** at a point on the skeleton is the radius of associated maximal ball.

The s-rep of a 2-D L-bracket is illustrated in Figure 3-1. A mathematical analysis of s-reps can be found in [Choi 97], [Calabi 68], [Sherbrooke 96].

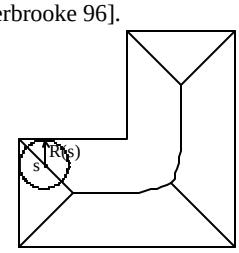

Figure 3-1: S-rep of an L-bracket.

We shall assume here that the skeletal representation of a 2-D solid can be computed using, for example, the techniques proposed in [Meshkat 87], [Srinivasan 87], [Ramanathan 02]. Techniques for 3-D computation of a s-rep may be found in [Sapidis 91], [Hoffman 94], [Turkiyyah 97], [Etzion 99], [Etzion 02].

3.1 S-Voronoi Decomposition

The theory developed in this paper is restricted to geometrically complex thin solids whose skeletal branches are of dimension 'n-1' and terminate at the boundary. Polygons and polyhedrons, for example, exhibit this property [Blum 78], [Nackman 82]. Such solids posses a convenient *S-Voronoi decomposition* discussed below.

On the other hand solids such as the one illustrated in Figure 3-2 are not considered here since one of the skeletal branches terminates in the interior of the domain. We expect to extend the theory to such solids in a forthcoming paper.

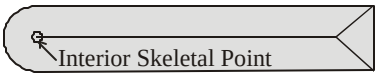

Figure 3-2: Interior skeletal point.

Focusing our attention on thin 2-D solids, let $(x_i(s), h_i(s))$, $1 \le i \le N$ be the N skeletal branches of a solid, where s is the arc length parameter ranging from 0 to l_i, the length of the skeletal branch. Further, let $R_i(s)$, $1 \le i \le N$ be the associated radius functions. Given a triple $(x_i(s), h_i(s), R_i(s))$ we define the following.

Define $a_i(s)$ to be the angle made by the tangent at $(x_i(s), h_i(s))$ to the global x axis, i.e.,

$$(\cos a_i, \sin a_i) \equiv \left(\frac{dx_i}{ds}, \frac{dh_i}{ds} \right) \equiv (x_{i,s}, h_{i,s})$$

Further, let $q_i(s)$ be the angle between the tangent vector, and the vector to the nearest boundary point. One can show that [Blum 78]:

$$q_i(s) = -\cos^{-1}\left(\frac{dR_i}{ds} \right)$$

Figure 3-3 illustrates a skeletal branch that is a bisector of two boundary segments, and the definition of a and q.

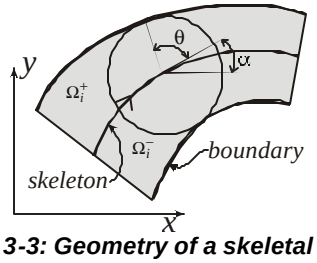

Figure 3-3: Geometry of a skeletal curve.

One can now associate two sets Ω_i^+ and Ω_i^- with each skeletal triple $(x_i(s), h_i(s), R_i(s))$ as follows:

$$\Omega_i^+ \equiv \left\{ \begin{matrix} x_i^+(s,k) = x_i + kR_i \cos(q_i + a_i) \\ y_i^+(s,k) = h_i + kR_i \sin(q_i + a_i) \end{matrix} \right\} \qquad \textbf{(3-1)}$$

$$0 \le s \le l_i; 0 \le k < 1$$

$$\Omega_i^- \equiv \left\{ \begin{matrix} x_i^-(s,k) = x_i + kR_i \cos(-q_i + a_i) \\ y_i^-(s,k) = h_i + kR_i \sin(-q_i + a_i) \end{matrix} \right\} \qquad \textbf{(3-2)}$$

$$0 \le s \le l_i; 0 \le k < 1$$

The sets Ω_i^+ and Ω_i^- lie on the left and right side, respectively, of a directed skeletal branch, as illustrated in Figure 3-3. Equations (3-1) and (3-2) are transformations from $\Psi_i = \{(s,k) \mid 0 \le s \le l_i, 0 \le k < 1\}$ to $\Omega_i^{\pm}$.

If none of the skeletal branches terminate in the interior, then one can show that the solid can be expressed via the following *S-Voronoi decomposition*:

$$\Omega = \bigcup_i \left(\Omega_i^+ + \Omega_i^- \right) \qquad \textbf{(3-3)}$$

On the other hand, if there are internal terminal points for a skeleton, then the decomposition has additional terms:

$$\Omega = \bigcup_i \left(\Omega_i^+ + \Omega_i^- \right) + \bigcup_k \Omega_k^0 \qquad \textbf{(3-4)}$$

We use the term S-Voronoi decomposition to distinguish it from the standard *Voronoi* decomposition [Srinivasan 87], the latter being a coarser version of the former. For example, Figure 3-4 illustrates the difference between the two for a rectangle.

(a) S-Voronoi decomposition

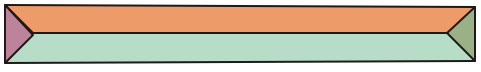

(b) Voronoi decomposition

Figure 3-4: S-Voronoi versus Voronoi decomposition.

Observe in Figure 3-4a that the S-Voronoi decomposition consists of 10 sub-domains, 2 sub-domains per skeletal branch. On the other hand, Figure 3-5b consists of 4 sub-domains, one per boundary segment.

Figure 3-5a illustrates the S-Voronoi decomposition of the dovetail consisting of 26 sub-domains. Figure 3-5b is a detailed view of Figure 3-5a about the left reentrant corner.

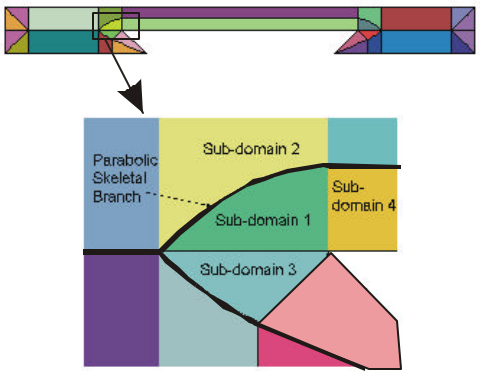

Figure 3-5: S-Voronoi decomposition of dovetail.

We shall assume here that the solid can be decomposed per Equation (3-3). If such is the case, then the boundary of the solid can also be decomposed as:

$$\partial\Omega = \bigcup_i \left(\Gamma_i^+ + \Gamma_i^-\right) \qquad \textbf{(3-5)}$$

where the two boundary curves $\Gamma_i^+(s)$ and $\Gamma_i^-(s)$ are obtained by setting $k = 1$ in Equations (3-1) and (3-2):

3.2 Jacobian Transformation

For transformations given by Equations (3-1) & (3-2), one may define standard Jacobians matrices [Bronshtein 85] that are employed in Section 4 of this paper:

$$J_i^{\pm}(sk) \equiv \begin{bmatrix} x_{i,s}^{\pm} & y_{i,s}^{\pm} \\ x_{i,k}^{\pm} & y_{i,k}^{\pm} \end{bmatrix} \qquad \textbf{(3-6)}$$

By definition, we have:

$$\begin{Bmatrix} U_{,s} \\ U_{,k} \end{Bmatrix}_i^{\pm} = J_i^{\pm} \begin{Bmatrix} U_{,x} \\ U_{,y} \end{Bmatrix}_i \qquad \textbf{(3-7)}$$

One can show that the determinant of the Jacobian is given by:

$$\left|J_i^{\pm}(s,k)\right| = \left|\pm R_i \sin q_i - kR_i(\pm q_{i,s} + a_{i,s})\right| \qquad \textbf{(3-8)}$$

The determinant will be employed in Section 4 in the transformation of area integrals between the (x,y) space and the (s,k) space. For polygons, the expression for the determinant can be vastly simplified by observing that a skeletal branch is one of three types summarized in Table 3-1 [Kim 95]. For each of the 3 types, the functions $q_{i,s}$ and $a_{i,s}$ appearing in Equation (3-8) simplify significantly, as summarized in Table 3-1 below.

Boundary Segments	**Skeletal Branch**	$a_{,s}$	$q_{,s}$
Line-line	Line-segment	0	0
Point-point	Line-segment	0	$\dfrac{\sin q}{R(s)}$
Point-line	Parabola	$\dfrac{\sin q}{2R(s)}$	$\dfrac{\sin q}{2R(s)}$

Table 3-1: Types of skeletal branches.

Finally, one can show that the Jacobian transformation defined per Equation (3-6) is invertible, i.e., the determinant is non-zero, in the interior of a domain. Thus, we have:

$$\begin{Bmatrix} U_{,x} \\ U_{,y} \end{Bmatrix}_i = \left(J_i^{\pm}\right)^{-1} \begin{Bmatrix} U_{,s} \\ U_{,k} \end{Bmatrix}_i^{\pm}$$

4. PROPOSED METHOD

In this section, we propose a generalized Kantorovich method for a variational formulation, using the variational statement of the Poisson's equation as a vehicle:

$$\textit{Minimize } \Pi(U) = \frac{1}{2}\int_0^l \int_{-h}^{h} \left(U_{,x}^2 + U_{,y}^2 - 2kU\right) dydx \qquad \textbf{(4-1)}$$

Subject to: $U = \hat{u}(\Gamma)$ for $(x,y) \in \partial\Omega$

The proposed method consists of the following steps.

Step-1: The first step is to compute the skeletal representation of the solid, and to express the solid as an S-Voronoi decomposition as in Equation (3-3). We assume that this can be carried out using one of technique proposed in [Meshkat 87] or [Etizon 99]. Due to the decomposition, the above minimization problem simplifies to:

$$\textit{Minimize } \sum_i \left(\Pi_i^{\pm}\left(U_i^{\pm}\right)\right)$$

where each term of the integral is of the form:

$$\Pi_i^{\pm}(U_i^{\pm}) = \begin{cases} \dfrac{1}{2}\iint\limits_{\Omega_i^{\pm}} \left[\left(U_{i,x}^{\pm}\right)^2 + \left(U_{i,y}^{\pm}\right)^2\right] dxdy \\ -\iint\limits_{\Omega_i^{\pm}} kU_i^{\pm} dxdy \end{cases} \qquad \textbf{(4-2)}$$

Step-2: The next step is to exploit the Jacobian transformation described in Section 3, to make a variable change $(x,y) \to (s,k)$ in Equation (4-2):

$$\Pi_i^{\pm}(U) = \begin{cases} \dfrac{1}{2}\int_0^{l_i}\int_0^1 \left(\overline{U}_i^{\pm}\right)^T \left(J_i^{\pm}\left(J_i^{\pm}\right)^T\right)^{-1} \overline{U}_i^{\pm}{}_i \left|J_i^{\pm}\right| dkds \\ -\int_0^{l_i}\int_0^1 kU_i^{\pm}\left|J_i^{\pm}\right| dkds \end{cases} \qquad \textbf{(4-3)}$$

$$\overline{U}_i^{\pm} = \begin{Bmatrix} U_{i,s}^{\pm} \\ U_{i,k}^{\pm} \end{Bmatrix}$$

We then define a set of generalized Kantorovich trial functions $U_i^{\pm}(s,k)$ that satisfy:

- Admissibility criterion
- Completeness criterion
- Conformance criterion
- Essential boundary conditions.

These requirements are identical to the ones imposed on finite element trial functions to ensure convergence [Strang 73], and are discussed below.

Admissibility: For the Poisson problem, the admissibility criterion states that the trial functions must be at least C^0 continuous across the boundaries of adjacent sub-domains in the *(x, y)* space. In Figure 3-5, sub-domain 1 is adjacent to sub-domains 2, 3 and 4. The trial functions defined in region 1 must therefore be at least C^0 continuous with the trial functions in 2, 3 and 4.

Observe that there are two types of adjacency. The first type (type-1) involves regions that share a common skeletal branch; the adjacency between regions 1 and 2 is of this type. Since a skeletal branch corresponds to $k = 0$ in Equations (3-1) and (3-2) type-1 adjacency requires that $U_i^+(s,0) = U_i^-(s,0)$.

On the other hand, in a type-2 adjacency, neighboring regions (example: 1 and 3) do not share a common skeletal branch but a common branch-point. This corresponds to $s = 0$ or $s = l_i$ in Equations (3-1) and (3-2), leading to compatibility conditions that describe how unknown functions defined on one skeletal branch are related to unknown functions over neighboring skeletal branches.

Completeness: Next consider the completeness criterion. Recall that a polynomial $g(k)$ is *complete* up to order m, if $g(k)$ contains $k^0, k^1, ..., k^m$. We impose a similar condition with respect to the thickness variable k on $U_i^{\pm}(s,k)$

Conformance: In the posed problem, the requirement for *conforming* trial functions is the same as the admissibility, i.e., the trial functions must be at least C^0 continuous across the boundaries of adjacent domains.

Boundary Conditions: Finally, $U_i^{\pm}(s,k)$ must satisfy *essential boundary conditions* on $\Omega_i^{\pm}$. Let $w_i^{\pm}(s)$ is the Dirichlet boundary condition on the boundary curve $\Gamma_i^{\pm}(s)$. The trial functions must therefore satisfy $U_i^{\pm}(s,1) = w_i^{\pm}(s)$

Trial Functions of type C^0: Consider the following trial functions, where $\{u_i(s)\}$ are unknown functions:

$$U_i^+(s,k) = \{u_i(s)(1-k) + w^+(s)k\} \text{ in } \Omega_i^+ \qquad \textbf{(4-4a)}$$

$$U_i^-(s,k) = \{u_i(s)(1-k) + w^-(s)k\} \text{ in } \Omega_i^- \qquad \textbf{(4-4b)}$$

One can verify that $U_i^{\pm}(s,k)$ satisfy all the above requirements (additional compatibility conditions must be imposed on $u_i(s)$ at branch points).

Trial Functions of type C^1: While the above trial functions meet the necessary requirements, better convergence can be expected if higher order continuity is imposed. For example, one can show that the following trial functions satisfy C^1 continuity:

$$U_i^+(s,k) = \begin{Bmatrix} u_i(s)(1-k^2) + \\ R\begin{Bmatrix} u_{i,s}\cos q + \\ q_i(s)\sin q \end{Bmatrix}(k-k^2) + \\ w^+(s)k^2 \end{Bmatrix} \text{ in } \Omega_i^+ \qquad \textbf{(4-5a)}$$

$$U_i^-(s,k) = \begin{Bmatrix} u_i(s)(1-k^2) + \\ R\begin{Bmatrix} u_{i,s}\cos q - \\ q_i(s)\sin q \end{Bmatrix}(k-k^2) + \\ w^-(s)k^2 \end{Bmatrix} \text{ in } \Omega_i^- \qquad \textbf{(4-5b)}$$

where $\{u_i(s), q_i(s)\}$ are unknown functions (compatibility conditions must be imposed on $\{u_i(s), q_i(s)\}$ at branch-points in order to have C^1 continuity for type-2 adjacency). Henceforth, we assume that the trial functions for the Poisson's equation are of type C^1 and are given by Equations (4-5a) and (4-5b).

Step-3: The next task is to substitute Equations (4-5a) and (4-5b) in Equation (4-3) and carry out a symbolic integration over the thickness variable k. As stated earlier, the task is vastly simplified since $U_i^{\pm}(s,k)$ involves low order polynomials. This task was executed using Mathematica™, a symbolic software package.

Once k is eliminated, the problem reduces to solving for $\{u_i(s), q_i(s)\}_{i=1}^N$ in:

$$Minimize \quad \Pi(U) = \sum_i \left(\Pi_i^{\pm}\left(u_i, u_{i,s}, u_{i,ss}, q_i, q_{i,s}\right)\right) \qquad \textbf{(4-6)}$$

subject to compatibility conditions at branch points.

Step-4: The final step is to apply a finite element procedure to minimize Equation (4-6) in an approximate sense using finite element approximation is standard [Shames 85]. We do not discuss the details here, except to note that we employ a Hermitian approximation of $u_i(s)$ and a linear approximation of $q_i(s)$.

5. NUMERICAL EXPERIMENTS

In the previous section, we enforced all the required conditions to ensure convergence of the proposed method. In order to study the accuracy of the proposed method, we consider a few field problems whose exact solutions are known. In addition, a few problems with no known closed-form solutions are also considered, and the results are compared to finite element solutions.

Recall that the Kantorovich method consists of two distinct approximation stages (Figure 1-2):

- Stage 1: Approximation via Kantorovich trial functions
- Stage 2: Approximation via finite element trial functions.

Each stage introduces an approximation error, referred to as stage-1 and stage-2 error. Depending on the problem, one

or both errors may be present. We measure the total numerical error using a pair of normalized L_∞ errors:

$$E_u = \frac{\max|u - \hat{u}|}{\max|u|} \;;\; E_q = \frac{\max|q - \hat{q}|}{\max|q|}$$

Experiment 1

The first numerical experiment involves solving the Laplace equation $\nabla^2 U(x, y) = 0$ over 2 convex solids: (a) a rectangle of length 1 and height 0.1, (b) an equilateral triangle of side 1. Dirichlet boundary conditions are specified and their values are such that the exact solution is a quadratic field "$U(x, y) = (x^2 - y^2) + 0.2(x + y)$".

Note that for convex solids, the geometric transformation between (s,k) space and (x, y) space, given by Equations (3-1) and (3-2), is linear. Thus the quadratic Kantorovich trial functions of Equation (4-5) and (4-5) are sufficient to capture the field exactly, i.e., one would expect the stage-1 error to be theoretically zero.

Further, in the finite element approximation, we have employed a quadratic approximation of $\hat{u}(s)$ and a linear approximation of capture $\hat{q}(s)$. Thus stage-2 error is also expected to be theoretically zero. Both these expectations are confirmed in Table 5-1.

$U(x,y) = \begin{Bmatrix}(x^2 - y^2) + \\ 0.2(x + y)\end{Bmatrix}$ **#Finite Elements** ~5	E_u	E_q
Rectangle	10^{-12}	10^{-11}
Triangle	10^{-12}	10^{-11}

Table 5-1: Normalized errors for Experiment 1.

The computed solution $\hat{u}(s)$ over the skeleton of the triangle is illustrated in Figure 5-1. This experiment suggests the generality of the proposed technique. In contrast, a 'mid-element' based Kantorovich method is inconceivable for the triangle.

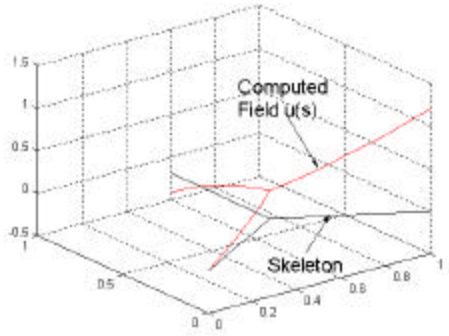

Figure 5-1: Computed solution over the skeleton.

Experiment 2

The next set of numerical experiments is similar to the first except that the exact solution is a Laplacian field "$U(x, y) = (x^3 - 3xy^2)$" over a rectangle of length 1 and height 0.1. We would expect to see stage-1 inaccuracy since the exact field is cubic while the approximating Kantorovich functions are quadratic. Stage-2 inaccuracy is expected to diminish with increasing number of elements. The normalized errors are summarized in Table 5-2. As expected, the errors diminish with increased number of elements, but never reach zero due to the presence of stage-1 error.

$U(x,y) = (x^3 - 3xy^2)$ **Rectangle (1x 0.1)**	E_u	E_q
#Finite Elements = 5	$5e^{-4}$	0.0211
#Finite Elements =13	$2.73e^{-5}$	0.0022
#Finite Elements = 23	$7.46e^{-6}$	$6e^{-4}$
#Finite Elements = 80	$6e^{-6}$	$1.05e^{-4}$
#Finite Elements = 200	$6e^{-6}$	$0.75e^{-4}$

Table 5-2: Normalized errors for Experiment 2.

Experiment 3

The third set of numerical experiment involves solving the Poisson's equation $\nabla^2 U(x, y) = -2$ over two non-convex solids (a) dovetail (Figure 2-4), and (b) a modified L-bracket (see Figure 5-2). Dirichlet boundary conditions are specified and their values are such that the exact solution is the Poisson field "$U(x, y) = -(x^2 + y^2)/2$".

Figure 5-2: A modified L-bracket.

The normalized errors are summarized in Table 5-3. The major contributor to the total error is stage-1. Observe that geometrically complex domains can be handled with equal ease.

Field: $-(x^2 + y^2)/2$ **#Finite elements**: 100	E_u	E_q
Dovetail	10^{-3}	10^{-2}
L-bracket	10^{-4}	10^{-2}

Table 5-3: Normalized errors for Experiment 3.

The computed solution over the modified L-bracket is illustrated in Figure 5-3.

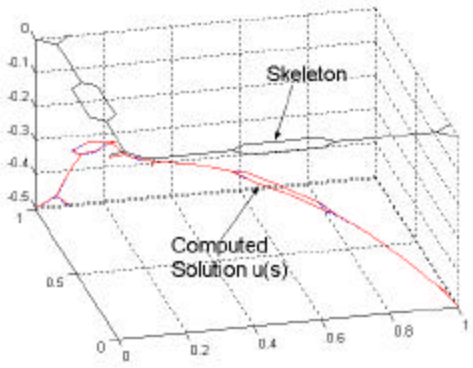

Figure 5-3: Computed solution on the skeleton of a modified L-bracket.

Experiment 4

The final set of numerical experiments involves computing torsional stiffness for various 2-D cross-sections. Closed-form solutions typically do not exist for such problems, barring a few exceptions. We assume here that Saint Venant's torsional assumptions hold true [Pilkey 02], [Chou 92]. For solids without holes, the problem reduces to solving $\nabla^2 j = -2$ in Ω and $j = 0$ in $\partial\Omega$, where j is the Prandtl's function … then computing the torsional stiffness given by $J = 2\int j \, d\Omega$.

Note that this experiment goes beyond just computing the two unknown functions $\hat{u}(s)$ and $\hat{q}(s)$ over the skeletal functions in that an integral of the 2-D solution over the entire domain must be computed.

We first consider the simple case of a thin rectangle whose torsional stiffness is known in closed-form. Figure 5-4 illustrates the computed Prandtl's function j over the skeleton of a rectangle of dimensions $L = 1, H = 0.05$.

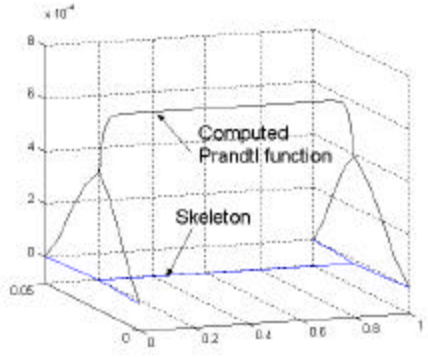

Figure 5-4: Prandtl's function j over the skeleton of a thin rectangle.

The exact, computed and St. Venant's estimate for the stiffness of a rectangle for 2 different aspect ratios are summarized in Table 5-4.

	Exact	***Proposed method #Elements =20***	***Proposed method #Elements =200***	***St. Venant's Estimate***
L=1; H=0.1	$3.123e^{-4}$	$3.0228e^{-4}$ (96.8%)	$3.076e^{-4}$ (98.5%)	$3.333e^{-4}$ (106.7%)
L=1; H=0.05	$4.035e^{-5}$	$3.9105e^{-5}$ (96.9%)	$4.001e^{-5}$ (99.1%)	$4.1667e^{-5}$ (103.2%)

Table 5-4: Torsional stiffness estimates for a rectangle.

Further examples appear in Table 5-5. St. Venant's estimate of the torsional stiffness is implicitly based on a mid-element representation; it leads to fairly accurate estimate stiffness for solids such as the rectangle and I-beam, but is inaccurate, as one would expect, for geometrically complex solids such as the dovetail

	2-D FEM Estimate	***#Finite Elements =100***	***St. Venant's Estimate***
I-Beam	$2.4208e^{-9}$	$2.4009e^{-9}$ (99.1%)	$2.395e^{-9}$ (98.9%)
Dovetail	$1.40112e^{-4}$	$1.3832e^{-4}$ (98.7%)	$1.875e^{-4}$ (133.1%)

Table 5-5: Torsional stiffness estimates for irregular geometry.

6. INCLUSION OF SINGULARITIES

In Sections 4 and 5 we used polynomials of k as trial functions – Equations (4-5a) and (4-5b) – to approximate an unknown field $U(s,k)$. Polynomials are sufficient if the field is sufficiently smooth or if only a global property of the field is desired. However, elliptic fields often exhibit singularities at the boundary that must be captured to predict, for example, failure of a stressed member.

The most common source of a singularity is the reflex or reentrant corner where the internal angle between two adjacent boundary edges exceeds 180^0. Figure 6-1 illustrates an example of a reentrant corner with an interior angle of a.

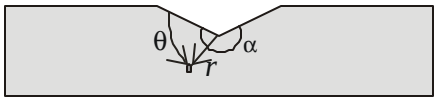

Figure 6-1: Singularity at a reentrant corner.

The nature of the singularity near a reentrant corner depends on the boundary conditions on the adjacent edges, and can be determined *a priori* up to an unknown constant. For example, let a field $U(x,y)$ satisfy the Poisson's equation over the domain in Figure 6-1, and let zero Dirichlet boundary conditions be specified over the entire domain. Then the first term of the singularity near the

reentrant corner of Figure 6-1 in polar coordinates is given by [Strang 73]:

$$U(r,q) = Kr^{\frac{p}{a}} \sin\left(\frac{qp}{a}\right)$$

where K is an unknown constant to be determined.

Unfortunately, polynomial trial functions cannot capture such singularities accurately. We propose here a simple strategy by augmenting polynomial functions with explicit singularity functions; this is similar to how singularities are handled in dassic finite element analysis [Strang 73]. The proposed strategy is as follows:

1. First create an artificial 'singularity region' of radius e centered about the reentrant corner, as illustrated in Figure 6-2.
2. Then represent the field in the e-region by a singularity function, and elsewhere, by polynomial trial functions as before.
3. Finally enforce C^0 or C^1 continuity, as appropriate, along the common boundary of the e-region.

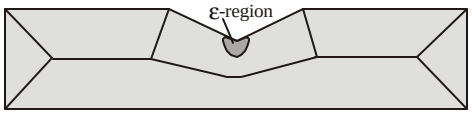

Figure 6-2: Isolation of the e-region

At the present time, we have not implemented the above strategy, and expect to do so in the future.

7. CONCLUSIONS

The preciseness and algorithmic nature of the proposed method leads to a high degree of automation and accuracy. Standard solid modeling, finite element and graph theoretical concepts are sufficient, i.e., 'special' modeling techniques used in mid-element based techniques are not required. The proposed method permits use of singularity functions if desired.

On the other hand, there are two significant challenges associated with the proposed method: (1) it requires the computation of a skeletal representation; while this is known to be a hard problem, especially in 3-D, recent research, example, [Etizon 02], is promising, and (2) the skeleton is 'sensitive' to small changes or representational inaccuracies in the boundary [Rezayat 96], and may require 'smoothening' or de-featuring [Donaghy 96].

8. REFERENCES

[Armstrong 94] Armstrong, C. G., "Modeling Requirements for Finite-Element Analysis", *Computer Aided Design*, vol. 26, no. 7, July 1994.

[Armstrong 95] Armstrong, C. G., Robinson, D. J., McKeag, R. M., Li, T. S., Bridgett, S. J., Donaghy, R. J., McGleenan, C. A., "Medials for Meshing and More", *Proceedings, 4th International Meshing Roundtable*, Sandia National Laboratories, Albuquerque, Oct 1995.

[Armstrong 98] Armstrong, C. G., Bridgett, S. J., Donaghy, R. J., McCune, McKeag, R. M., R. W., Robinson, D. J., "Techniques for Interactive and Automatic Idealization of CAD Models", *Numerical Grid Generation in Computational Field Simulations, Ed. M. Cross., B. K. Soni, J. F. Thompson, J. Hauser, P. R. Eiseman*, Proceedings of the 6th International Conference, held at the University of Greenwich, pp.643-662, July 1998.

[Armstrong 99] Armstrong, C. G., Bradley, B., "Design Optimization By Incremental Modification Model", *Proceedings, 8th International Meshing Roundtable*, South Lake Tahoe, CA, U.S.A., pp.293-298, October 1999.

[Babuska 94] Babuska, I., Lee, I., Schwab, C., "On the a posteriori estimation of the modeling error for the heat conduction in a plate and its use for adaptive hierarchical modeling", *Applied Numerical Mathematics*, 14, pp. 5-21, 1994.

[Blum 78] Blum, H., and Nagel, R. N., "Shape Description using Weighted Symmetric Axis Features", *Pattern Recognition*, vol. 10, pp. 167-180, 1978.

[Bronshtein 85] Bronshtein, I. N., and Semendyayev, K. A., **Handbook of Mathematics**, Van Nostrand Reinhold Company, New York, NY, 1985.

[Calabi 68] Calabi, L, and Hartnett, W. E., "Shape Recognition, Prairie Fires, Convex Deficiencies and Skeletons", *American Mathematical Monthly*, pp. 335-342, April 1968.

[Choi 97] Choi, H. I.,Choi, S. W., Moon, H. P., "Mathematical Theory of Medial Axis Transform", *Pacific Journal of Mathematics*, Vol. 181, No. 1, pp. 57-88, 1997.

[Chou 92] Chou, P. C, Pagano, N. J., **Elasticity: Tensor, Dyadic and Engineering Approaches**, Dover Publications, 1992.

[Donaghy 96] Donaghy, R. J., Cune, W. M., Bridgett, S. J., Armstrong, C. G., Robinson, D. J., McKeag, R. M., "Dimensional Reduction of Analysis Models", *5th International Meshing Roundtable*, Sandia National Laboratories, pp. 307-320, 1996.

[Etzion 99] Etzion, M., Rappoport, A., "Computing the Voronoi Diagram of a 3-D Polyhedron by Separate Computation of its Symbolic and Geometric Parts", *Proceedings, Fifth Symposium on Solid Modeling*, Ann Arbor, MI, pp. 167-178, 1999.

[Etzion 02] Etzion, M., Rappoport, A., "Computing Voronoi Skeletons of a 3-D Polyhedron by space subdivision", *Computational Geometry*, 21, pp. 87-120, 2002.

[Hoffman 94] Hoffman, C. M., "How to construct the skeleton of CSG Objects", *Computer-Aided Surface Geometry and Design*, Oxford University Press, edited by Bowyer, A., pp. 421- 437, 1994.

[Kantorovich 64] Kantorovich, L. V., Krylov, V. I., **Approximate Methods of Higher Analysis**, Interscience, New York, 1964.

[Kim 95] Kim, D-S, Hwang, I-K, Park, B-J, "Representing the Voronoi diagram of a simple polygon using

rational quadratic Bezier curves", *Computer Aided Design*, Vol. 27, No 8, 1995.

[Madureira 99] Madureira, A. L., "Asymptotics and Hierarchical Modeling of Thin Domains", Ph.D. thesis, Department of Mathematics, The Pennsylvania State University, August 1999.

[Meshkat 87] Meshkat, S. N., and Sakkas, C. M., "Voronoi diagram for multiply-connected polygonal domains II: Implementation and application", *IBM Journal of Research and Development*, vol. 31, no. 3, pp. 373-381, May 1987.

[Monaghan 98] Monaghan, D. J., "Coupling 1D Beams to 3D Bodies", *Proceedings, 7th International Meshing Roundtable*, Sandia National Lab, pp.285-293, October 1998.

[Nackman 82] Nackman, L. R., "Curvature Relations in Three-Dimensional Symmetric Axes", *Computer Graphics and Image Processing*, 20, pp. 43-57, 1982.

[Onodera 01] Onodera, M., Nishigaki, I., "Medial Surface Generation Technique for CAD-CAE Coupling", *Transactions of the Japan Society for Computational Engineering and Science*, August 2001.

[Pilkey 94] Pilkey, W. D., Wunderlich,W., **Mechanics of Structures: Variational and Computational Methods**, CRC Press, 1994.

[Pilkey 02] Pilkey, W. D., **Analysis and Design of Elastic Beams: Computational Methods**, John Wiley & Sons, 2002.

[Price 95] Price, M.A., Armstrong, C. G., "Hexahedral Mesh Generation by Medial Surface Subdivision: Part I, Solids With Convex Edges", *International Journal for Numerical Methods in Engineering*, Wiley, Vol 38, Num 19, pp.3335-3359, October 1995.

[Ramanathan 02] Ramanathan, M., Gurumoorthy, B., "Constructing medial axis transform of planar domains with curved boundaries", *Computer-Aided Design*, 35, PP. 619-632, 2002.

[Reddy 84] Reddy, J. N., **Energy and Variational Methods in Applied Mechanics**, John Wiley and Sons, New York, 1984.

[Reissner 85] Reissner, E., "Reflections on the Theory of Elastic Plates", Journal of Applied Mechanics, vol. 38, no. 11, pp. 1453-1464, 1985.

[Rezayat 96] Rezayat, M., "Midsurface abstraction from 3D solids models: general theory and applications", *Computer Aided Design*, Vol. 28, No. 11, pp. 905-915, 1996.

[Sapidis 91] Sapidis, N. S., Perucchio, R., "Domain Delanuay Tetrahedrization of Arbitrarily Shaped Curved Polyhedra Defined in a Solid Modeling System", *Proc. Symposium on Solid Modeling Foundations and CAD/CAM Applications*, Ed. J. Rossignac and J. Turner, pp. 465-480, June 1991.

[Shames 85] Shames, I. H., Dym, C. L., **Energy and Finite Element Methods in Structural Mechanics**, McGraw Hill, New York, 1985.

[Sheffer 98] Sheffer A., Etzion, M., Rappoport, A., Bercovier, M., "Hexahedral mesh generation using Voronoi skeletons", *Proceedings of the Seventh International Meshing Roundtable*, Michigan, October 1998.

[Sherbrooke 96] Sherbrooke, E. C., Patrikalakis, N. M., Wolter, F-E., "Differential and Topological Properties of Medial Axis Transforms", *Graphical Models and Image Processing*, Vol. 58, No. 6, pp. 574-592, 1996.

[Shim 01] Shim, K. W., Monaghan, D. J., Armstrong, C. G., "Mixed Dimensional Coupling in Finite Element Stress Analysis", *Proceedings, 10th International Meshing Roundtable*, Sandia National Laboratories, pp.269-277, October 7-10 2001.

[Srinivasan 87] Srinivasan, V., and Nackman, L. R., "Voronoi diagram for Multiply-Connected Polygonal Domains I: Algorithm", *IBM Journal of Research and Development*, vol. 31, no. 3, pp. 361-372, May 1987.

[Strang 73] Strang, G., Fix, G. J., An Analysis of the Finite Element Method, Prentice-Hall, 1973.

[Tam 91] Tam, T. K. H, Armstrong, C. G., "2D Finite Element Mesh Generation by Medial Axis Subdivision", *Advances in Engineering Software*, Elsevier, Vol 56, Num 13, pp.313-324, 1991.

[Turkiyyah 97] Turkiyyah G. M., Storti, D., Ganter, M., Chen, H., Vimawala, M., "An accelerated triangulation method for computing the skeletons of free-form solid models", *Computer Aided Design*, 29 (1), pp. 5-19, 1997.

[Vogelius 81] Vogelius, M., Babuska, I., "On a Dimensional reduction Method I. The Optimal Selection of Basis Functions", *Mathematics of Computation*, Volume 37, Issue 155, pp. 31-46, 1981.

[Wang 00] Wang, C. M., Reddy, J. N., Lee, K. H., Shear **Deformable Beams and Plates: Relationship to Classical Solutions**, Elsevier Science, 2000.